J. Fluid Mech. (1991), *vol.* 222, *pp.* 501–524
Printed in Great Britain

The trapping and scattering of topographic waves by estuaries and headlands

By THOMAS F. STOCKER† AND E. R. JOHNSON
Department of Mathematics, University College London, Gower Street, London WC1E 6BT, UK

(Received 22 October 1988 and in revised form 3 December 1989)

This paper extends recent theoretical work on sub-inertial trapped modes in bays to consider trapping of energy in the neighbourhood of estuary mouths on coastal shelves. The qualitative form of the theoretical predictions accords well with recent observations on the Scotian Shelf that show energy trapped near the Laurentian Channel at a frequency higher than that of the propagating waves on the shelf.

The trapping and scattering of shelf waves is modelled for a shelf–estuary or shelf–headland system by considering barotropic waves in a straight, infinite channel with an attached rectangular estuary or interrupted by a rectangular headland. Taking the depth to increase exponentially with distance from the coast and expanding in cross-shelf modes reduces the problem to a system of real linear algebraic equations.

Trapped modes with frequencies above the cutoff frequency of propagating waves are found near the mouth of the estuary. Waves propagating towards the estuary are strongly scattered and, for particular frequencies, incident energy can be either perfectly transmitted or totally reflected. An incident wave can be in resonance with the estuary causing energy to penetrate the estuary. Bounds on the frequencies of trapped and resonant solutions are given and allow an easy modal interpretation.

If the frequency of an incident wave is sufficiently high, waves cannot propagate past a headland. Energy at these frequencies can however tunnel through the region and appear as an attenuated wave on the far side. For particular frequencies all energy passes the headland and none is reflected. For headlands long compared with the incident wave, transmission coefficients for single-mode scattering follow from spatially one-dimensional wave mechanics.

1. Introduction

Topographically trapped waves are the predominant low-frequency component of ocean currents near many coasts. A review of observational evidence for such waves is given by Mysak (1980) who also summarizes theoretical results for waves that propagate along continental shelves with unchanged offshore profile but decay away from the coast. Recent theoretical work (Stocker & Hutter 1987; Stocker 1988; Johnson 1989*a*; Stocker & Johnson 1989) points to the further possibility of geographically localized regions of wave motion with modes decaying exponentially both out to sea and along the shelf away from the wave region. These results are supported by the recent observations on the Scotian Shelf near the Laurentian Channel (figure 1*a*), reported by Schwing (1989). Schwing notes significant energy in

† On leave from Department of Meteorology, McGill University, Montreal, Canada.

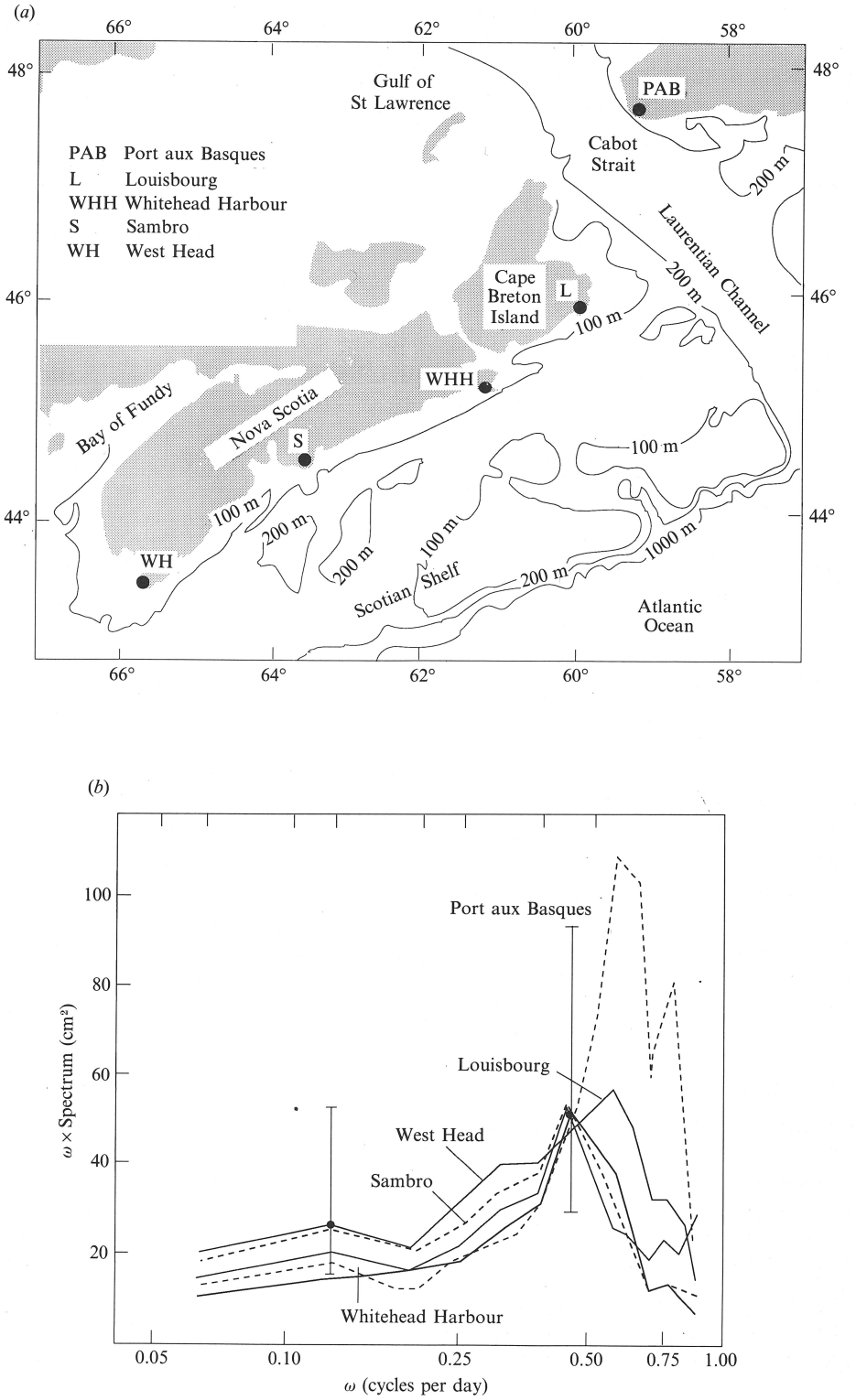

FIGURE 1. For caption see facing page.

the neighbourhood of the estuary mouth at a frequency slightly higher than those found on the shelf (figure 1*b*), finding further that energy at this frequency does not propagate effectively. It is the purpose of the present paper to extend the earlier theoretical results to a geometry more closely modelling a shelf interrupted by an estuary to obtain qualitative results for comparison with these and other observations. As the methods used yield results for the complementary geometry of a shelf interrupted by a headland, these too are noted briefly.

The simplest discussion of coastally trapped waves is in the context of the non-divergent barotropic conservation of potential vorticity. Buchwald & Adams (1968) demonstrate that solutions model well current measurements off South-East Australia. Middleton, Foster & Foldvik (1987) model similarly shelf waves in the southern Weddell Sea and Schwing (1989) also models his waves as barotropic. Thus the barotropic equation is introduced in §2 and solved for a coast interrupted by a rectangular estuary or headland. The features are taken to be of size comparable with the shelf width and hence scatter significant energy. Solutions for slow or small variations in shelf width or depth are given by Grimshaw (1977) and for smoothly varying shelves by Webster (1987). Scattering by abrupt changes in width has been discussed by Wilkin & Chapman (1987) who however confine their attention to widening shelves where no short waves are back-scattered, and thus preclude trapped modes. It is shown in Johnson (1989*b*, *c*, 1990) in the low-frequency limit that at a narrowing, energy is back-scattered in short waves and dissipated in narrow layers on the incident side of obstacles if the flow is weakly dissipative or carried far from the scattering region if the flow is inviscid.

Following Wilkin & Chapman (1987) and Middleton & Wright (1988), the geometry of a shelf abutting a flat open ocean is modelled by a channel with a rigid wall at the shelf–ocean junction. Following Buchwald & Adams (1968) the depth is taken to increase exponentially from the wall so the governing equation reduces to a Helmholtz equation. The model is thus closely related to that for surface gravity waves discussed in similar geometries by Buchwald & Williams (1975). In their problem however trapped modes are precluded as the fundamental mode is propagating at all frequencies and so carries energy away from any region. The present problem is reduced to an algebraic eigenvalue problem by expanding in cross-shelf modes. The convergence of this expansion and its numerical approximation is considered in §3.1. In §3.2 bounds on the eigenfrequencies are obtained following Johnson (1989*a*) and used to assign mode numbers to, and to interpret, the trapped modes of an estuary. Modes scattered by an estuary or headland are discussed in §§3.3 and 3.4. Conformally similar geometries to which the results can be applied are noted in §3.5. A summary of the results is given in §4 together with a more detailed comparison of the results to the observations of Schwing (1989) and a brief discussion of the effects and importance of the free surface, dissipation and stratification.

FIGURE 1. (*a*) The position of tide-gauge stations whose readings are reported in Schwing (1989). (*b*) The autospectra (variance preserved) of low-pass-filtered time series for coastal bottom pressure and 95% confidence intervals given in Schwing (1989). The strongest response at Port aux Basques, in Cabot Strait, and at Louisbourg, on the shelf near the mouth of the Laurentian Channel, occurs at a frequency above that of the strongest propagating wave at Whitehead Harbour, Sambro and West Head on the shelf away from the channel mouth.

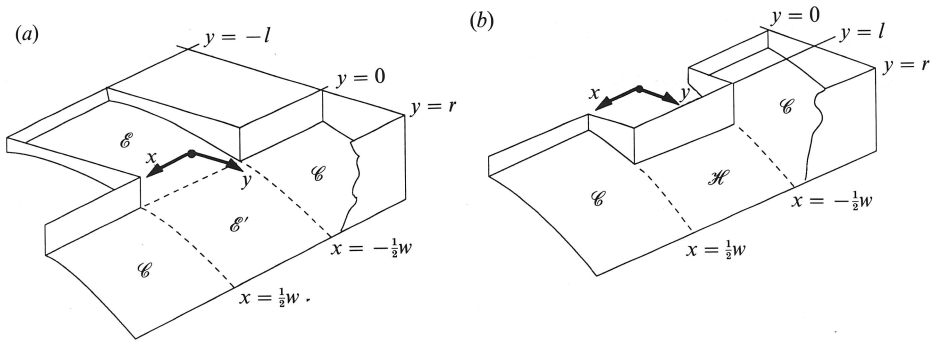

FIGURE 2. (*a*) An estuary $\mathscr{E}$ ($-\frac{1}{2}w \leqslant x \leqslant \frac{1}{2}w$, $-l \leqslant y \leqslant 0$) with estuary mouth $\mathscr{E}'$ ($-\frac{1}{2}w \leqslant x \leqslant \frac{1}{2}w$, $0 \leqslant y \leqslant r$) and a channel shelf $\mathscr{C}$ ($|x| \geqslant \frac{1}{2}w, 0 \leqslant y \leqslant r$). (*b*) A headland ($-\frac{1}{2}w \leqslant x \leqslant \frac{1}{2}w, 0 \leqslant y \leqslant l$) interrupting a shelf $\mathscr{C}$. The channel abreast the headland is denoted by $\mathscr{H}$.

2. Solution procedure

2.1. *Governing equations*

Non-divergent, barotropic shelf waves on the f-plane can be described by the non-dimensionalized conservation equation of potential vorticity,

$$\nabla\cdot(H^{-1}\nabla\Psi_t)+\hat{z}\cdot(\nabla\Psi\wedge\nabla H^{-1})=0, \quad \text{in} \quad \mathscr{D}, \tag{2.1}$$

$$\hat{n}\cdot(\hat{z}\wedge\nabla\Psi)=0, \quad \text{on} \quad \partial\mathscr{D}, \tag{2.2}$$

where Ψ is the mass transport stream function, H the local fluid depth, $\hat{z}$ a vertical unit vector, $\hat{n}$ an outward normal vector, and ∇ the horizontal gradient operator, and the scale for the non-dimensional time t is f^{-1}. Condition (2.2) states the vanishing mass transport across the boundary $\partial\mathscr{D}$ of the domain $\mathscr{D}$.

Consider the geometry and Cartesian coordinates sketched in figure 2. The straight shelf is interrupted by an estuary (figure 2*a*) or a headland (figure 2*b*) of length l and width w. The frequencies and structure of waves propagating along a rectilinear shelf adjacent to an open ocean and in bays adjoining shelves are shown in Johnson (1989*a*) to be governed by a simple variational principle with their behaviour lying between extremes obtained using two limiting forms for the boundary conditions at the open boundary. In the present geometry these limiting conditions become the requirement that either $\partial\Psi/\partial x$ or Ψ vanishes on $y = r$. The former corresponds to the long-wave limit and the latter to a rigid boundary and the short-wave limit. The solutions are qualitatively similar and thus in the present work we choose the rigid boundary condition throughout as this leads to explicit forms of the dispersion relation. This is also the condition used by Wilkin & Chapman (1987) and Middleton & Wright (1988).

Let the depth profile be given by

$$H(y) = \mathrm{e}^{2b(y-r)}.$$

Equation (2.1) then has solutions of the form

$$\Psi = \mathrm{Re}\{\mathrm{e}^{-\mathrm{i}\sigma t}\psi\},$$

provided

$$\psi_{xx}+\psi_{yy}-2b\psi_y-\mathrm{i}\frac{2b}{\sigma}\psi_x=0. \tag{2.3}$$

Note that if $\psi(x,y)$ satisfies (2.3) then so also does $\psi^*(-x,y)$, where $(\,)^*$ denotes the complex conjugate. Introduce

$$\psi(x,y) = \mathrm{e}^{by+\mathrm{i}(b/\sigma)x}\phi(x,y), \tag{2.4}$$

so (2.3) gives the purely real system

$$\left.\begin{aligned} \phi_{xx}+\phi_{yy}+b^2(1/\sigma^2-1)\,\phi = 0, \quad \text{in} \quad \mathscr{D}, \\ \phi = 0, \quad \text{on} \quad \partial\mathscr{D}. \end{aligned}\right\} \tag{2.5}$$

This has solutions of the form

$$\phi_n = (a_n \sin \kappa_n x + b_n \cos \kappa_n x) \sin \frac{n\pi y}{r} \quad (n = 1, 2, \ldots), \tag{2.6}$$

where

$$\kappa_n = \left[b^2\left(\frac{1}{\sigma^2}-1\right)-\left(\frac{n\pi}{r}\right)^2\right]^{\frac{1}{2}}, \quad \sigma = \frac{b}{[\kappa_n^2+b^2+(n\pi/r)^2]^{\frac{1}{2}}}, \tag{2.7}$$

a dispersion relation for $\kappa_n(\sigma)$. It follows that the nth transverse mode propagates provided

$$\sigma < \sigma_n^{\mathscr{C}} = \frac{b}{[b^2+(n\pi/r)^2]^{\frac{1}{2}}}. \tag{2.8}$$

If $\sigma > \sigma_n^{\mathscr{C}}$ the nth mode decays exponentially with distance from the estuary or headland on a scale $|\kappa_n|^{-1}$. For $\sigma < \sigma_1^{\mathscr{C}}$ incident shelf waves can interact with the wave field in the estuary or abreast the headland leading to strong scattering.

2.2. *Trapped modes in an estuary*

At frequencies greater than $\sigma_1^{\mathscr{C}}$ all channel modes are evanescent and no energy is carried away from the estuary. Modes can still propagate in the estuary, however, and solutions are therefore trapped.

For $\sigma > \sigma_1^{\mathscr{C}}$, a solution of (2.5), odd in x and decaying as $|x| \to \infty$, is

$$\left.\begin{aligned} \phi_0^{\mathscr{E}} &= \sum_{n=1}^{\infty} a_n S_n(x) \sin n\pi\left(\frac{y+l}{r+l}\right) \quad (0 \leqslant x \leqslant \tfrac{1}{2}w), \\ \phi_0^{\mathscr{C}} &= \sum_{n=1}^{\infty} c_n E_n(x) \sin \frac{n\pi y}{r} \quad (x \geqslant \tfrac{1}{2}w), \end{aligned}\right\} \tag{2.9}$$

for the domains $\mathscr{E} \cup \mathscr{E}'$ and $\mathscr{C}$, respectively; and for $x < 0$

$$\phi_0(x, y) = -\phi_0(-x, y),$$

where

$$\left.\begin{aligned} S_n(x) &= \begin{cases} \sinh(\alpha_n x)/\sinh(\tfrac{1}{2}\alpha_n w) & (\alpha_n^2 > 0) \\ \sin(\hat{\alpha}_n x)/\sin(\tfrac{1}{2}\hat{\alpha}_n w) & (\hat{\alpha}_n^2 > 0) \end{cases} \\ \hat{\alpha}_n^2 &= -\alpha_n^2, \\ \alpha_n^2 &= [n\pi/(r+l)]^2 - b^2(1/\sigma^2-1), \\ E_n(x) &= \mathrm{e}^{-\lambda_n(x-\frac{1}{2}w)}, \\ \lambda_n &= [-\kappa_n^2]^{\frac{1}{2}}. \end{aligned}\right\} \tag{2.10}$$

The function $\phi_0^{\mathscr{E}}$ is odd and satisfies the boundary condition at the estuary end $y = -l$ and the channel wall $y = r$; $\phi_0^{\mathscr{E}}$ vanishes along the channel walls $y = 0, r$. Note that $\phi_0 = 0$ on $x = 0$ and ϕ_0 therefore also represents a solutions in a channel with a terminating estuary zone.

The geometry contains two singular points ($x = \pm\frac{1}{2}w, y = 0$), where the velocity field assumes infinite values. Sufficiently close to these points the topography is locally flat and (2.5) reduces to Laplace's equation, with wave functions ϕ behaving as $\rho^{\frac{2}{3}}$, where ρ is the distance from the singularity. The Fourier coefficients a_n and c_n thus can be expected to have the asymptotic behaviour (Lighthill 1958, pp. 43, 72)

$$a_n, c_n \sim n^{-\frac{5}{3}} \quad (n \gg 1). \tag{2.11}$$

This is verified in the numerical solutions of §3.1, confirming that (2.9) converges absolutely and is bounded everywhere.

An even solution can be similarly constructed by replacing $S_n(x)$ in (2.10) by $C_n(x)$ with

$$C_n(x) = \begin{cases} \cosh(\alpha_n x)/\cosh(\tfrac{1}{2}\alpha_n w) & (\alpha_n^2 > 0), \\ \cos(\hat{\alpha}_n x)/\cos(\tfrac{1}{2}\hat{\alpha}_n w) & (\hat{\alpha}_n^2 > 0). \end{cases}$$

Both odd and even functions solve the problem individually.

The solutions of both subdomains match at $x = \frac{1}{2}w$, i.e.

$$\phi^{\mathscr{E}'}(\tfrac{1}{2}w, y) = \phi^{\mathscr{C}}(\tfrac{1}{2}w, y) \quad (0 \leqslant y \leqslant r), \tag{2.12a}$$

$$\phi^{\mathscr{E}}(\tfrac{1}{2}w, y) = 0 \quad (-l \leqslant y \leqslant 0). \tag{2.12b}$$

A further condition is provided by the continuity of the velocity field expressed in terms of $\nabla\phi$. From (2.11) it follows that $a_n \alpha_n, c_n \lambda_n \sim n^{-\frac{2}{3}}$ for $n \gg 1$ and hence the derivatives of the expansions (2.9) do not necessarily converge at $y = 0$. This singular behaviour can be avoided by introducing the modified stream functions $\tilde{\phi}(x, y) \equiv \phi(x, y) f(y)$, where $f(y)$ is an arbitrary, differentiable function with $\lim_{y \to 0}[f(y)/y^{\frac{1}{3}}] = 0$. In order to preserve the orthogonality properties of $\phi^{\mathscr{C}}$ we choose

$$\tilde{\phi}^{\mathscr{E}} = \phi^{\mathscr{E}} \sin \pi y/r, \quad \tilde{\phi}^{\mathscr{C}} = \phi^{\mathscr{C}} \sin \pi y/r$$

and demand

$$\frac{\partial \tilde{\phi}^{\mathscr{E}'}}{\partial x} = \frac{\partial \tilde{\phi}^{\mathscr{C}}}{\partial x} \quad (0 \leqslant y \leqslant r). \tag{2.12c}$$

For $0 < y < r$, condition (2.12c) on $\tilde{\phi}_x$ is equivalent to requiring the continuity of ϕ_x across $x = \frac{1}{2}w$. It is a weaker condition in that boundedness of ϕ or ϕ_x at the singularities is not demanded. The modified functions lead to absolutely convergent Fourier series whose coefficients can be expected to have the asymptotic behaviour $\tilde{a}_n, \tilde{c}_n \sim n^{-\frac{8}{3}}$ for $n \gg 1$. This is also verified in the numerical solutions of §3.1.

The modified expansions are

$$\left.\begin{aligned} \tilde{\phi}_0^{\mathscr{E}}(x, y) &= \sum_{n=1}^{\infty} a_n S_n(x) \sin\frac{\pi y}{r} \sin\frac{n\pi(y+l)}{r+l}, \\ \tilde{\phi}_0^{\mathscr{C}}(x, y) &= \sum_{n=1}^{\infty} \tilde{c}_n \tilde{E}_n(x) \cos\frac{(n-1)\pi y}{r}, \end{aligned}\right\} \tag{2.13}$$

and the modified coefficients $\tilde{c}_n \tilde{E}_n(x)$ are related to $c_n E_n(x)$ by

$$\left.\begin{aligned} \tilde{c}_n \tilde{E}_n &= \sum_{k=1}^{\infty} P_{nk} c_k E_k, \\ P_{nk} &= \tfrac{1}{2}(\delta_{nk} - \delta_{n,k+2}), \end{aligned}\right\} \quad (n, k = 1, 2, \ldots), \tag{2.14}$$

where δ_{nk} is the Kronecker delta. Equations (2.12a, b) then imply

$$\sum_{n=1}^{\infty} a_n \sin\frac{n\pi(y+l)}{r+l} = \begin{cases} \displaystyle\sum_{n=1}^{\infty} c_n \sin\frac{n\pi y}{r} & (0 \leqslant y \leqslant r), \\ 0 & (-l \leqslant y \leqslant 0), \end{cases} \tag{2.15}$$

The functions $\sin[m\pi(y+l)/(r+l)]$, $m = 1, 2, \ldots$ vanish at $y = -l$ and $y = r$ and form an orthogonal, complete set on $[-l, r]$. Operating with

$$\int_{-l}^{r} \mathrm{d}y \sin[m\pi(y+l)/(r+l)] \quad (m = 1, 2, \ldots)$$

on both sides of (2.15) yields

$$\tfrac{1}{2}(r+l)\,a_m = \sum_{n=1}^{\infty} G_{mn}\,c_n, \tag{2.16}$$

where

$$G_{mn} = \int_0^r \mathrm{d}y \sin\frac{m\pi(y+l)}{r+l}\sin\frac{n\pi y}{r} = \begin{cases} \dfrac{n}{\pi r}\dfrac{1}{\left(\dfrac{n}{r}\right)^2-\left(\dfrac{m}{r+l}\right)^2}\sin\dfrac{m\pi l}{r+l} & \left(\dfrac{n}{r}\neq\dfrac{m}{r+l}\right), \\ \tfrac{1}{2}r(-1)^{m+n} & \left(\dfrac{n}{r}=\dfrac{m}{r+l}\right). \end{cases}$$

From (2.12*c*)

$$\sum_{n=1}^{\infty} a_n S_n'(\tfrac{1}{2}w)\sin\frac{\pi y}{r}\sin\frac{n\pi(y+l)}{r+l} = \sum_{n=1}^{\infty}\tilde{c}_n\tilde{E}_n'(\tfrac{1}{2}w)\cos\frac{(n-1)\pi y}{r+l}, \tag{2.17}$$

with $(\,)' \equiv \partial/\partial x$.

Using now the complete set $\cos[(m-1)\pi r/r]$, $m = 1, 2, \ldots$ and operating with

$$\int_0^r \mathrm{d}y \cos[(m-1)\pi y/r] \quad (m = 1, 2, \ldots)$$

on both sides of (2.17) gives

$$\sum_{n=1}^{\infty}\tilde{G}_{nm}S_n'(\tfrac{1}{2}w)\,a_n = \tfrac{1}{2}r(1+\delta_{m1})\tilde{E}_m'(\tfrac{1}{2}w)\,\tilde{c}_m. \tag{2.18}$$

The modified matrix $\tilde{\boldsymbol{G}}$ can be obtained from $\boldsymbol{G}$ via

$$\tilde{G}_{nm} = \sum_{k=1}^{\infty}\tilde{P}_{mk}G_{nk}, \tag{2.19}$$

where

$$\tilde{P}_{mk} = P_{mk}+\tfrac{1}{2}\delta_{k1}\delta_{mk}. \tag{2.20}$$

The tilded quantities in (2.18) are now replaced using (2.14), (2.19) and (2.20) to yield

$$\sum_{n=1}^{\infty}\sum_{k=1}^{\infty}\tilde{P}_{mk}G_{nk}S_n'a_n = \tfrac{1}{2}r\sum_{k=1}^{\infty}\tilde{P}_{mk}E_k'c_k.$$

The matrix $\tilde{\boldsymbol{P}}$ has an explicit inverse, and substitution of $\boldsymbol{c}$ in (2.16) results the linear homogeneous system

$$\sum_{n=1}^{\infty}A_{mn}a_n = 0, \tag{2.21}$$

with

$$A_{mn} = S_n'\sum_{k=1}^{\infty}G_{mk}G_{nk}/E_k' - \tfrac{1}{4}r(r+l)\,\delta_{mn}.$$

Non-trivial solutions exist provided

$$\det\boldsymbol{A} = 0.$$

This equation determines the eigenfrequencies of the odd modes trapped in the estuary. In order to obtain the whole spectrum of eigenfrequencies, including the fundamental mode, the even problem must also be solved. This follows by solving a system similar to (2.21) where in A_{mn} the S_n' are replaced by C_n'.

For a numerical solution the expansion (2.9) is truncated to order N, reducing the problem to finding the zeros of the determinant of a $N \times N$ real matrix. If the problem were solved in the complex ψ-representation without using the symmetry property the system would be complex of dimension $8N \times 8N$ in the worst case. Using symmetry and the real ϕ-representation allows a substantial saving and larger truncation orders can be chosen when better spatial resolution is required.

2.3. *Propagating modes scattered by an estuary*

At frequencies less than $\sigma_1^{\mathscr{C}}$ propagating modes in the channel can carry energy away from the estuary. Consider the simplest case of the frequency range $\sigma_2^{\mathscr{C}} < \sigma < \sigma_1^{\mathscr{C}}$ so the fundamental mode, with transverse order $n = 1$, is the sole propagating mode in the channel. The selection of a particular incident wave, say a long wave propagating from $x = -\infty$ towards the estuary, destroys the symmetry of the problem and both even and odd solutions are required to give the correct energy flux.

The odd solution can be written

$$\left.\begin{aligned} \phi_0^{\mathscr{E}}(x,y) &= \sum_{n=1}^{\infty} a_n S_n(x) \sin\frac{n\pi(y+l)}{r+l} \quad (0 \leqslant x \leqslant \tfrac{1}{2}w), \\ \phi_0^{\mathscr{C}}(x,y) &= c_1 \cos(\kappa_1(x-\tfrac{1}{2}w)+\gamma) \sin\frac{\pi y}{r} + \sum_{n=2}^{\infty} c_n E_n(x) \sin\frac{n\pi y}{r} \quad (x \geqslant \tfrac{1}{2}w), \end{aligned}\right\} \tag{2.22}$$

where c_1 and γ are the as yet undetermined amplitude and phase of a standing fundamental mode. The matching conditions for ϕ_0 and $\partial\tilde{\phi}_0/\partial x$ at $x = \frac{1}{2}w$ yield

$$\left.\begin{aligned} \tfrac{1}{2}(r+l)\, a_m &= G_{m1} \cos\gamma c_1 + \sum_{n=2}^{\infty} G_{mn}\, c_n, \\ \sum_{n=1}^{\infty} G_{nm} S_n'(\tfrac{1}{2}w)\, a_n &= \tfrac{1}{2}r(1+\delta_{m1}) \tilde{E}_m'(\tfrac{1}{2}w)\, \tilde{c}_m, \end{aligned}\right\} \tag{2.23}$$

where $\tilde{E}_1'(\frac{1}{2}w) = -\kappa_1 \sin\gamma$ and $\tilde{E}_n'(\frac{1}{2}w)$, $n \geqslant 2$ are given by (2.10). Combining (2.23) and substituting for the tilded quantities as before gives

$$\sum_{n=1}^{\infty} C_{mn}\, c_n = 0, \tag{2.24}$$

with

$$C_{m1} = \cos\gamma \sum_{k=1}^{\infty} G_{km}\, G_{k1}\, S_k' + \tfrac{1}{4}r(r+l)\, \kappa_1 \sin\gamma\, \delta_{m1},$$

$$C_{mn} = \sum_{k=1}^{\infty} G_{km}\, G_{kn}\, S_k' - \tfrac{1}{4}r(r+l)\, E_m'\, \delta_{mn} \quad (n \geqslant 2),$$

where $\boldsymbol{C}$ depends on the unknown phase γ. Non-zero solutions require

$$\det \boldsymbol{C}(\gamma) = 0.$$

The phase γ appears in only the first column of $\boldsymbol{C}$, i.e.

$$C_{11} = g_1 \cos\gamma + h_1 \sin\gamma,$$
$$C_{m1} = g_m \cos\gamma \quad (m \geqslant 2),$$

where $\boldsymbol{g}$ and $\boldsymbol{h}$ are independent of γ. Expanding the determinant by the first column gives

$$\det \boldsymbol{C} = (g_1 \cos\gamma + h_1 \sin\gamma)\, C^{11} + \cos\gamma \sum_{k=2}^{\infty} g_k\, C^{k1},$$

where C^{k1} is the cofactor of C_{k1}. If $C^{11} = 0$ then $\gamma = \frac{1}{2}\pi$, otherwise γ is given explicitly as

$$\tan\gamma = -\sum_{k=1}^{\infty} g_k C^{k1}/h_1 C^{11}.$$

The even solution can be written as

$$\phi_{\mathrm{e}}^{\mathscr{E}}(x,y) = \sum_{n=1}^{\infty} b_n C_n(x) \sin\frac{n\pi(y+l)}{r+l} \quad (0 \leqslant x \leqslant \tfrac{1}{2}w),$$

$$\phi_{\mathrm{e}}^{\mathscr{C}}(x,y) = d_1 \cos(\kappa_1(x-\tfrac{1}{2}w)+\delta)\sin\frac{\pi y}{r} + \sum_{n=2}^{\infty} d_n E_n(x)\sin\frac{n\pi y}{r} \quad (x \geqslant \tfrac{1}{2}w),$$

and the system corresponding to (2.23) as

$$\sum_{n=1}^{\infty} D_{mn} d_n = 0, \tag{2.25}$$

where $\boldsymbol{D}$ is obtained from $\boldsymbol{C}$ by replacing S'_k and γ by C'_k and δ. The phase δ of the even standing wave mode is determined by

$$\det \boldsymbol{D}(\delta) = 0.$$

The even and odd standing modes can be linearly combined to give an incident long wave from $x = -\infty$. There is no incoming energy flux from $x = +\infty$ and hence

$$c_1 \mathrm{e}^{\mathrm{i}\gamma} + d_1 \mathrm{e}^{\mathrm{i}\delta} = 0. \tag{2.26}$$

The amplitudes of the incident, reflected and transmitted modes are given by

$$\left.\begin{aligned} A_{\mathrm{I}} &= -c_1 \mathrm{e}^{\mathrm{i}\gamma} + d_1 \mathrm{e}^{\mathrm{i}\delta}, \\ A_{\mathrm{R}} &= -c_1 \mathrm{e}^{-\mathrm{i}\gamma} + d_1 \mathrm{e}^{-\mathrm{i}\delta}, \\ A_{\mathrm{T}} &= c_1 \mathrm{e}^{-\mathrm{i}\gamma} + d_1 \mathrm{e}^{-\mathrm{i}\delta}. \end{aligned}\right\} \tag{2.27}$$

Reflection and transmission coefficients are conveniently defined as

$$R = |A_{\mathrm{R}}/A_{\mathrm{I}}|^2, \quad T = |A_{\mathrm{T}}/A_{\mathrm{I}}|^2,$$

and from (2.26) and (2.27)

$$R = \cos^2(\gamma-\delta), \quad T = \sin^2(\gamma-\delta), \tag{2.28}$$

satisfying the flux balance $R+T = 1$. Equation (2.28) demonstrates that in the case of a single propagating mode the important quantities describing the scattering process at the estuary are simply obtained by calculating the phases of the standing modes, i.e. by again finding the zeros of the determinant of the $N \times N$ matrices $\boldsymbol{C}$ and $\boldsymbol{D}$. The numerical procedures for the trapped mode frequencies and for the reflection coefficients are thus similar. Reflection and transmission coefficients can be calculated similarly when more propagating modes are present.

2.4. *Propagating modes scattered by a headland*

A similar analysis to that in §2.3 can be performed to investigate the scattering of shelf waves incident on a headland (figure 2*b*). Since the channel is narrower abreast the headland the cutoff frequency of propagating shelf waves is smaller than that in the channel, namely

$$\sigma_n^{\mathscr{H}} = b \Big/ \left[b^2 + \left(\frac{n\pi}{r-l}\right)^2\right]^{\frac{1}{2}} < \sigma_n^{\mathscr{C}},$$

and so trapped modes cannot occur. The changing wave properties cause strong scattering, however.

When incident shelf waves are evanescent abreast the headland, energy can still pass through and appear as a transmitted wave on the far side: energy tunnels through. It is the interaction of both exponentially decaying and growing headland modes that results in the tunnelled energy flux.

Consider the odd solution

$$\phi_o^{\mathscr{H}}(x,y) = \sum_{n=1}^{\infty} a_n S_n^{\mathscr{H}}(x) \sin\frac{n\pi(t-l)}{r-l} \quad (0 \leqslant x \leqslant \tfrac{1}{2}w),$$

where $\phi_o^{\mathscr{C}}$ is unchanged and given by (2.22) and $S_n^{\mathscr{H}}(x)$ follows from $S_n(x)$ by replacing α_n^2 by $(\alpha_n^{\mathscr{H}})^2 = b^2(1/\sigma^2-1)-(n\pi/(r-l))^2$ in (2.10). The matching conditions are

$$\begin{aligned} \phi^{\mathscr{H}}(\tfrac{1}{2}w,y) &= \phi^{\mathscr{C}}(\tfrac{1}{2},y) \quad && (l \leqslant y \leqslant r), \\ \phi^{\mathscr{H}}(\tfrac{1}{2}w,y) &= 0 && (0 \leqslant y \leqslant l), \\ \frac{\partial\tilde{\phi}^{\mathscr{H}}}{\partial x} &= \frac{\partial\tilde{\phi}^{\mathscr{C}}}{\partial x} && (l \leqslant y \leqslant r), \end{aligned}$$

with $\tilde{\phi} = \phi \sin[\pi(y-l)/(r-l)]$, implying the linear system

$$\left.\begin{aligned} \sum_{n=1}^{\infty} H_{mn}\, a_n &= \tfrac{1}{2}r(\delta_{m1}\cos\gamma + 1 - \delta_{m1})\, c_m, \\ \tfrac{1}{2}(r-l)(1+\delta_{m1})\,\tilde{S}_m^{\mathscr{H}\prime}(\tfrac{1}{2}w)\,\tilde{a}_m &= \sum_{n=1}^{\infty} \tilde{H}_{mn} E_n'(\tfrac{1}{2}w)\, c_n, \end{aligned}\right\} \tag{2.29}$$

where

$$(1+\delta_{m1})\,\tilde{a}_m \tilde{S}_m^{\mathscr{H}\prime} = \sum_{k=1}^{\infty} \tilde{P}_{mk}\, a_k S_k^{\mathscr{H}\prime},$$

$$\tilde{H}_{mn} = \sum_{k=1}^{\infty} \tilde{P}_{mk} H_{nk},$$

$$H_{mn} = \int_l^r dy \sin\frac{m\pi y}{r}\sin\frac{n\pi(y-l)}{r-l} = \begin{cases} \dfrac{n}{\pi(r-l)}\dfrac{1}{\left(\dfrac{n}{r-l}\right)^2-\left(\dfrac{m}{r}\right)^2}\sin\dfrac{m\pi l}{r} & \left(\dfrac{n}{r-l} \neq \dfrac{m}{r}\right), \\ \tfrac{1}{2}(r-l)(-1)^{m+n} & \left(\dfrac{n}{r-l} = \dfrac{m}{r}\right), \end{cases}$$

$$E_1'(\tfrac{1}{2}w) = -\kappa_1 \sin\gamma^{\mathscr{H}},$$

and $\tilde{P}_{mk}$ is given by (2.20). As in §2.3, system (2.29) reduces to

$$\sum_{n=1}^{\infty} C_{mn}^{\mathscr{H}}\, c_n = 0, \tag{2.30}$$

with

$$C_{m1}^{\mathscr{H}} = -\kappa_1 \sin\gamma^{\mathscr{H}} \sum_{k=1}^{\infty} H_{mk} H_{1k}/S_k^{\mathscr{H}\prime} - \tfrac{1}{4}r(r-l)\cos\gamma^{\mathscr{H}}\,\delta_{m1},$$

$$C_{mn}^{\mathscr{H}} = E_n' \sum_{k=1}^{\infty} H_{mk} H_{nk}/S_k^{\mathscr{H}\prime} - \tfrac{1}{4}r(r-l)\,\delta_{mn} \quad (n \geqslant 2).$$

Non-trivial solutions exist provided $\det \boldsymbol{C}(\gamma^{\mathscr{H}}) = 0$, determining the phase $\gamma^{\mathscr{H}}$. Notice that $\boldsymbol{C}^{\mathscr{H}}$ and $\boldsymbol{C}$ have similar structure and again the phase $\gamma^{\mathscr{H}}$ appears only in the first column of $\boldsymbol{C}^{\mathscr{H}}$, i.e.

$$\begin{aligned} C_{11}^{\mathscr{H}} &= g_1^{\mathscr{H}} \sin\gamma^{\mathscr{H}} + h_1 \cos\gamma^{\mathscr{H}}, \\ C_{m1}^{\mathscr{H}} &= g_m^{\mathscr{H}} \sin\gamma^{\mathscr{H}} \quad (m \geqslant 2), \end{aligned}$$

and $\boldsymbol{C}^{\mathscr{H}}$ is singular if

$$\cot\gamma^{\mathscr{H}} = -\sum_{k=1}^{\infty} g_k^{\mathscr{H}}(C^{\mathscr{H}})^{k1}/h_1^{\mathscr{H}}(C^{\mathscr{H}})^{11},$$

where $(C^{\mathscr{H}})^{k1}$ is the cofactor of $C_{k1}^{\mathscr{H}}$. Replacing $S_k^{\mathscr{H}'}$ by $C_k^{\mathscr{H}'}$ in (2.30) yields the system for the even solution and allows calculation of the phase $\delta^{\mathscr{H}}$. Following (2.26) and (2.27) the reflection and transmission coefficients for waves scattered by a headland are given by (2.28) with γ and δ replaced by $\gamma^{\mathscr{H}}$ and $\delta^{\mathscr{H}}$.

3. Results

3.1. *Convergence*

Numerical solutions of the linear systems (2.21), (2.24), (2.25) and (2.30) are obtained by truncating the expansions (2.9) and (2.13) to order N. Any error in matching the stream function and velocity fields across $x = \frac{1}{2}w$ is then orthogonal to all transverse modes $n \leqslant N$. Numerical convergence of the eigenfrequencies and the solutions with increasing N is demonstrated below.

As the derivation in §2.1 of the linear system rested on the assumption that the infinite series (2.9) and (2.13) converge absolutely, the Fourier coefficients of the solution must decay sufficiently rapidly. It was noted in §2.1 that the coefficients are dominated by the singular behaviour of the solution at $x = \pm\frac{1}{2}w$, $y = 0$. This led to the estimates that for large n the coefficients decay as $n^{-\beta}$, where $\beta = \frac{5}{3}$ for a_n and c_n and $\beta = \frac{8}{3}$ for $\tilde{c}_n$. Figure 3 shows that the calculated coefficients decay approximately according to $n^{-\beta}$ where $\beta = 1.65$ for a_n and c_n and $\beta = 2.75$ for $\tilde{c}_n$, in good agreement with the predicted values. As $\beta > 1$ in all cases, expansions (2.9) and (2.13) converge absolutely.

Now consider convergence with respect to N, i.e. convergence of the truncated solutions to the true solution. Table 1 gives converging eigenfrequencies of the first four trapped modes in the estuary. It is remarkable that the low-order approximation with $N = 2$ yields the first three eigenfrequencies with an error of less than 1 %. Table 2 displays converging reflection and transmission coefficients for increasing truncation order N. The three cases $R \approx T$, $R \ll T$ and $R \gg T$, for the estuary and the maximum transmission coefficient of tunnelled energy for two headlands are considered. All cases show convergence. For propagating modes, however, higher truncation orders must be selected to accurately predict the solutions.

3.2. *Trapped modes in an estuary*

It follows from (2.8) that the cutoff frequency of the estuary region $\mathscr{E} \cup \mathscr{E}'$ (figure 2*a*) is larger than the cutoff in the channel $\mathscr{C}$, i.e.

$$\sigma_n^{\mathscr{E}\mathscr{E}'} = \frac{b}{\left[b^2 + \left(\frac{n\pi}{r+l}\right)^2\right]^{\frac{1}{2}}} > \sigma_n^{\mathscr{C}} = \frac{b}{\left[b^2 + \left(\frac{n\pi}{r}\right)^2\right]^{\frac{1}{2}}}.$$

Within a certain frequency interval waves propagate in the estuary but their energy remains trapped because they are evanescent in the channel. In Johnson (1989*a*) bounds on the eigenfrequencies are given that allow identification of the modal structure of an eigensolution when the geometric parameters of the problem are known. These again prove useful in this study where the geometry is more complicated.

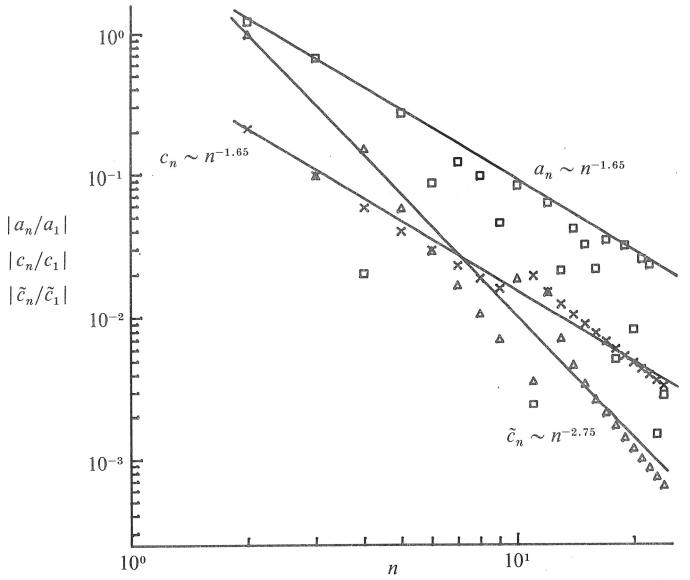

FIGURE 3. The modulus of the normalized coefficients of expansions (2.9) and (2.13) where the symbols □, × and △ denote a_n, c_n and $\tilde{c}_n$, respectively. The coefficients represent the fundamental trapped mode σ_{11} for $N = 24$, $b = 1$, $r = 1$, $w = 3$, $l = 1.3$ and $\sigma_{11} = 0.5081$. The dependence of the coefficients on n follows closely the behaviour indicated by the straight lines.

N	σ_{11}	σ_{21}	σ_{12}	σ_{22}
2	0.527931	0.392257	0.351693	0.312373
4	0.527189	0.390150	0.349858	0.308105
8	0.526868	0.389473	0.349594	0.307595
12	0.526823	0.389373	0.349552	0.307502
16	0.526780	0.389283	0.349519	0.307437
20	0.526761	0.389246	0.349507	0.307415
24	0.526751	0.389223	0.349499	0.307399

TABLE 1. Convergence of the eigenfrequencies of the first four modes trapped in the estuary. The parameters are $b = 1$, $r = 1$, $w = 3$ and $l = 1.5$.

	(*a*) Estuary			(*b*) Headland	
N	$R(\sigma = 0.280)$	$R(\sigma = 0.240)$	$R(\sigma = 0.208)$	$T_{\max}(\sigma = 0.275)$	$T_{\max}(\sigma = 0.188)$
2	0.154259	0.005352	0.046115	0.609378	0.153985
4	0.564242	0.022839	0.981784	0.577138	0.134540
8	0.591242	0.033515	0.997377	0.554871	0.128432
12	0.597065	0.036101	0.997430	0.554314	0.125878
16	0.600671	0.037869	0.997323	0.553435	0.125255
20	0.601659	0.038448	0.997383	0.552606	0.124777
24	0.602553	0.038901	0.997347	0.552796	0.124674

TABLE 2. (*a*) Convergence of the reflection coefficient for three frequencies of an incident fundamental wave scattered by an estuary of length $l = 1.5$. (*b*) Convergence of the maximum transmission coefficient of an incident fundamental wave tunnelling through a headland region of length $l = 0.1$ (left) and $l = 0.4$ (right). The other parameters are $b = 1$, $r = 1$ and $w = 1$.

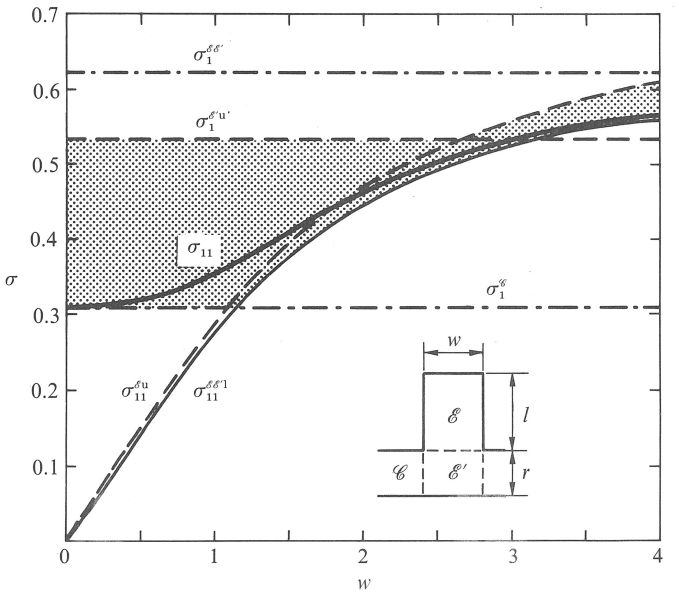

FIGURE 4. The fundamental eigenfrequency and bounds as a function of the estuary width. The frequencies $\sigma_1^{\mathscr{E}\mathscr{E}'}$ and $\sigma_1^{\mathscr{C}}$ are the cutoffs for a channel of width $l+r$ and r, respectively. The values $\sigma_{11}^{\mathscr{E}u}$ and $\sigma_1^{\mathscr{E}'u}$ are upper bounds for the subdomains $\mathscr{E}$ and $\mathscr{E}'$ and $\sigma_{11}^{\mathscr{E}\mathscr{E}'1}$ is the lower bound in the closed basin $\mathscr{E} \cup \mathscr{E}'$. The (1, 1)-mode thus lies in the shaded area. The parameters are $b = 1$, $r = 1$ and $l = 1.5$.

Let σ_{nm} be the eigenvalue of the (n, m)-mode, where n is the mode number in the x-direction (across estuary) and m the mode number in the y-direction (along estuary). The qualitative behaviour of the eigenvalues σ_{nm} with respect to w, the width of the channel, can be found by considering various bounds on σ_{nm}. A lower bound follows by taking the closed-basin limit of region $\mathscr{E} \cup \mathscr{E}'$, i.e.

$$\sigma_{nm}^{\mathscr{E}\mathscr{E}'1} = \frac{b}{\left[b^2 + \left(\frac{n\pi}{w}\right)^2 + \left(\frac{m\pi}{r+l}\right)^2\right]^{\frac{1}{2}}}.$$

The boundary conditions $\psi = 0$ on $y = -l$, $x = \pm w\frac{1}{2}$ and $\psi_y = 0$ on $y = 0$, give an upper bound on σ_{nm} in the subdomain $\mathscr{E}$ as

$$\sigma_{nm}^{\mathscr{E}u} = \frac{b}{\left[b^2 + \left(\frac{u\pi}{w}\right)^2 + \left(\frac{(m-\frac{1}{2})\pi}{l}\right)^2\right]^{\frac{1}{2}}}.$$

An upper bound in $\mathscr{E}'$ is obtained by taking $\psi = 0$ on $y = r$, $\psi_x = 0$ on $x = \pm\frac{1}{2}w$ and $\psi_y = 0$ on $y = 0$, thus

$$\sigma_m^{\mathscr{E}'u} = \frac{b}{\left\{b^2 + \left[\frac{(m-\frac{1}{2})\pi}{r}\right]^2\right\}^{\frac{1}{2}}}.$$

The largest eigenvalue σ_{11} thus satisfies

$$\max(\sigma_{11}^{\mathscr{E}\mathscr{E}'1}, \sigma_1^{\mathscr{C}}) \leqslant \sigma_{11} \leqslant \max(\sigma_{11}^{\mathscr{E}u}, \sigma_1^{\mathscr{E}'u}). \tag{3.1}$$

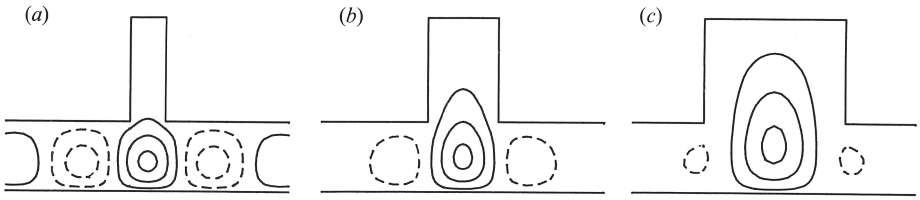

FIGURE 5. Streamlines of the trapped shelf wave mode σ_{11}. With increasing estuary width w wave motion gradually enters the estuary. The parameters are $N = 16$, $b = 1$, $r = 1$, $l = 1.5$: (a) $\sigma_{11} = 0.306$, $w = 0.5$, (b) $\sigma_{11} = 0.335$, $w = 1$, and (c) $\sigma_{11} = 0.457$, $w = 2$.

The upper bound holds because σ_{11} cannot exceed both upper bounds in the subdomains $\mathscr{E}$ and $\mathscr{E}'$. The lower bound follows since the (1, 1)-mode has no nodal line $y =$ constant. Inequality (3.1) defines the shaded area in figure 4. Note that σ_{11} is bounded by $\sigma_1^{\mathscr{E}'\mathrm{u}}$ rather than $\sigma_{11}^{\mathscr{E}\mathrm{u}}$ for smaller widths w of the estuary and approaches $\sigma_1^{\mathscr{C}}$. Inequality (3.1) also indicates that the trapped (1, 1)-mode is present for any values of w, b or l since $\sigma_{11} \geqslant \sigma_1^{\mathscr{C}}$.

Most of the wave activity is concentrated in the subdomain $\mathscr{E}$ and the activity in $\mathscr{E}$ decreases with decreasing w. A narrow estuary can cause a *trapped* shelf wave concentrated on the shelf around the mouth of the estuary, with frequency slightly higher than the cutoff of the shelf. The trapped mode decays exponentially in both directions. This is shown in figure 5 for three estuary widths.

Similar arguments lead to a description of the behaviour of higher-order modes. Consider the (2, 1)-mode which is bounded by

$$\max(\sigma_{21}^{\mathscr{E}\mathscr{E}'1}, \sigma_1^{\mathscr{C}}) \leqslant \sigma_{21} \leqslant \sigma_{11}.$$

The upper bound holds as σ_{11} is the largest eigenvalue by definition and the lower bound follows since the (2, 1)-mode has no nodal line $y =$ constant and its frequency exceeds the closed-basin limit in region $\mathscr{E} \cup \mathscr{E}'$. This area is shaded in figure 6(a) and the calculated value of σ_{21} is also given. Comparing figures 4 and 6(a) suggests that in the limit $w \to 0$ there is an infinite sequence of modes $(n, 1)$ trapped on the shelf. The exponential decay of the stream function away from the estuary mouth increases with increasing n.

A further point of interest is illustrated by the (1, 2)-mode. This mode has one node in the y-direction and no node in the x-direction. Bounds are given by

$$\max(\sigma_{12}^{\mathscr{E}\mathscr{E}'1}, \sigma_2^{\mathscr{C}}) \leqslant \sigma_{12} \leqslant \min(\sigma_2^{\mathscr{E}\mathscr{E}'}, \sigma_{11}).$$

The lower bound follows since there are fewer than two nodal lines $y =$ constant and the frequency must exceed the closed-basin limit of region $\mathscr{E} \cup \mathscr{E}'$. The upper bound holds by the definition of σ_{11}, and $\sigma_2^{\mathscr{E}\mathscr{E}'}$ is the open-basin limit. A further constraint is given by

$$\sigma_{12} < \max(\sigma_{11}^{\mathscr{E}\mathrm{u}}, \sigma_1^{\mathscr{C}}), \tag{3.2}$$

which again follows since there must be at least one nodal line $y =$ constant. These bounds give the shaded area in figure 6(b). The area crosses the cutoff $\sigma_1^{\mathscr{C}}$ of the channel, showing that the trapped mode (1, 2) starts to propagate on the shelf as w is decreased. It has been demonstrated in Stocker & Johnson (1989) that such a mode transforms into a *resonance* or, in this context, a leaky estuary mode. Inequality (3.2) further implies that the (1, 2)-mode is leaky for all values of w provided $l < \frac{1}{2}r$. Again, for narrow estuaries all the resonances $\sigma_{n2}, n = 1, 2, \ldots$, approach $\sigma_2^{\mathscr{C}}$ with wave

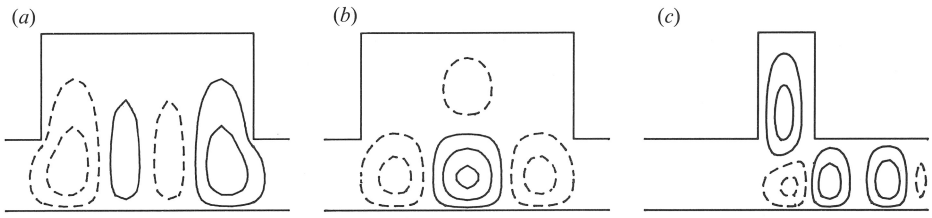

FIGURE 7. Streamlines of trapped modes, (*a*) and (*b*), and a resonance, (*c*). The parameters are $N = 16$, $b = 1$, $r = 1$, $l = 1.5$; and (*a*) $\sigma_{21} = 0.389$, $w = 3$, (*b*) $\sigma_{12} = 0.350$, $w = 3$, and (*c*) $\sigma_{12} = 0.226$, $w = 0.8$.

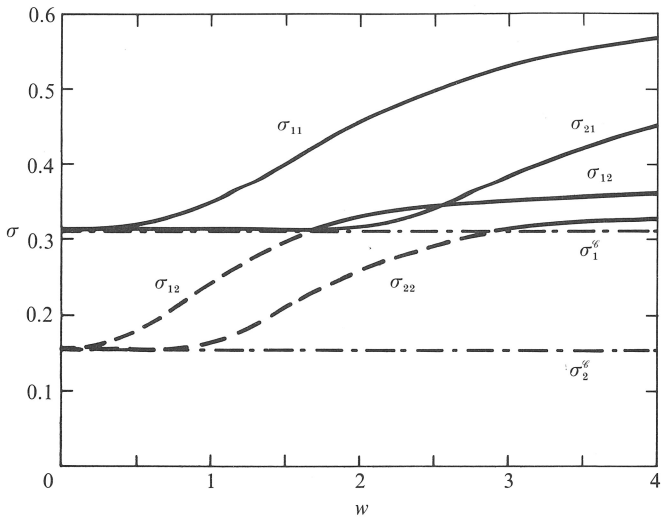

FIGURE 8. Eigenfrequencies of the four lowest modes as functions of the estuary width. Solutions are trapped for $\sigma > \sigma_1^{\mathscr{C}}$. For frequencies below the shelf cutoff the first transverse mode propagates and the trapped modes become resonances (dashed). The frequencies σ_{nm} are bounded by $\sigma_{nm} > \sigma_m^{\mathscr{C}}$. Parameters are given in figure 4.

summarizes these results for the four lowest modes. It is evident that the identification of the different modes would have been more difficult had the bounds not been used. The considerations in this section also allow the dependence of the eigenfrequencies on the parameters l, r and b, respectively describing the geometry and the topography, to be determined.

3.3. *Scattering by an estuary*

In this section attention is restricted to frequencies $\sigma_2^{\mathscr{C}} < \sigma < \sigma_1^{\mathscr{C}}$, so only the mode of lowest transverse order is propagating in the channel. A long shelf wave incident from $x = -\infty$ produces a short reflected and a long transmitted wave. The scattering depends on the geometry of the estuary and the frequency of the incident disturbance.

Figure 9(*a*) shows the reflection coefficient to be a strong function of the incident wave frequency. In general most incident energy is transmitted except near certain discrete frequencies where it is totally reflected. For increasing width of the estuary the frequency associated with a given perfect reflection increases. Also, the number of frequencies at which the incident wave is perfectly reflected increases with the width of the scattering region. Figure 9(*b*) shows R for three values of the length of

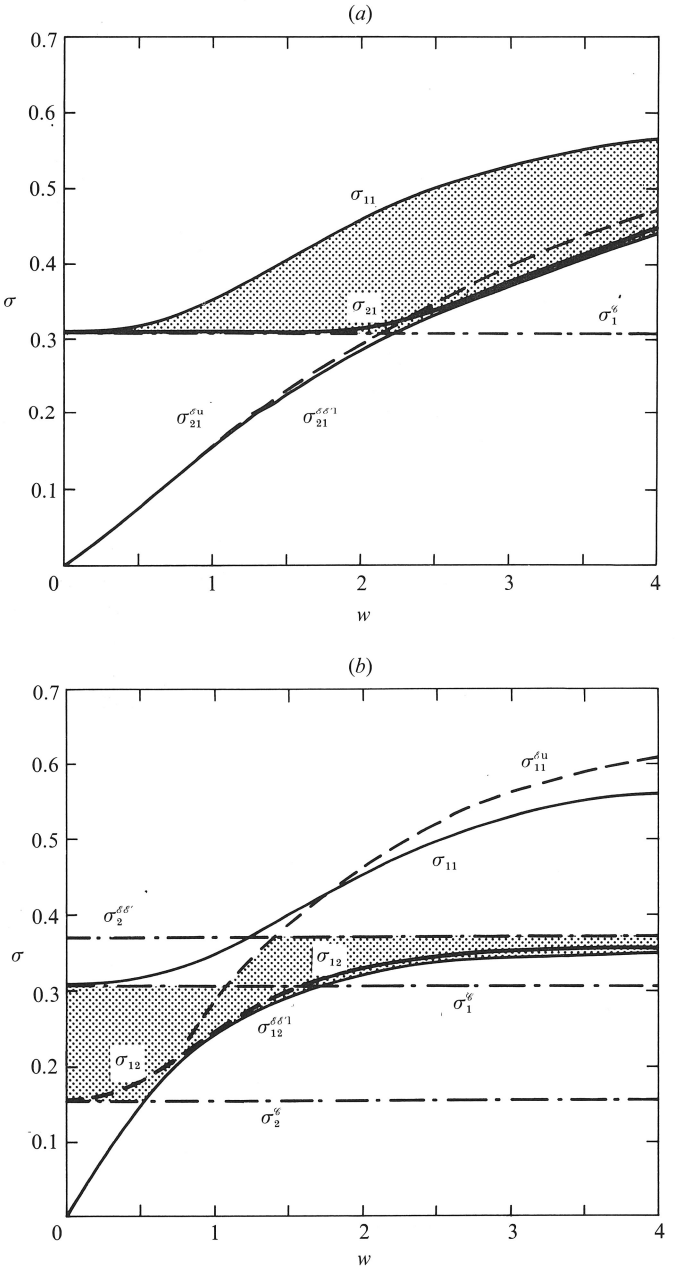

FIGURE 6. The eigenfrequency (*a*) σ_{21} and (*b*) σ_{12} and bounds as functions of w for $b = 1$, $r = 1$ and $l = 1.5$. For $\sigma^{12} < \sigma_1^G$ the mode starts to propagate on the shelf; the trapped mode becomes a resonance (dashed bold in (*b*)). The shaded region gives the combination of the bounds.

activity mainly on the shelf. Stream functions of modes (2, 1) and (1, 2) are displayed in figure 7: (*a*) and (*b*) show trapped modes and (*c*) displays the resonance obtained by decreasing the estuary width of (*b*).

The regions of parameter space corresponding to particular eigenfrequencies have been delineated by applying various bounds on the different eigenmodes. Figure 8

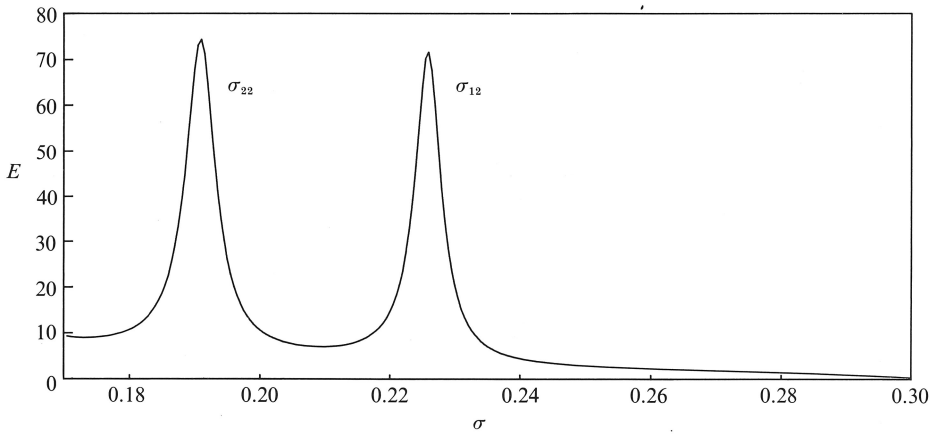

FIGURE 11. The time-averaged kinetic energy integrated over the estuary region $\mathscr{E} \cup \mathscr{E}'$ as a function of the frequency of the incident wave. The two resonances can be attributed to eigenmodes in the estuary; $N = 12$, $b = 1$, $r = 1$, $l = 1.5$, $w = 0.8$.

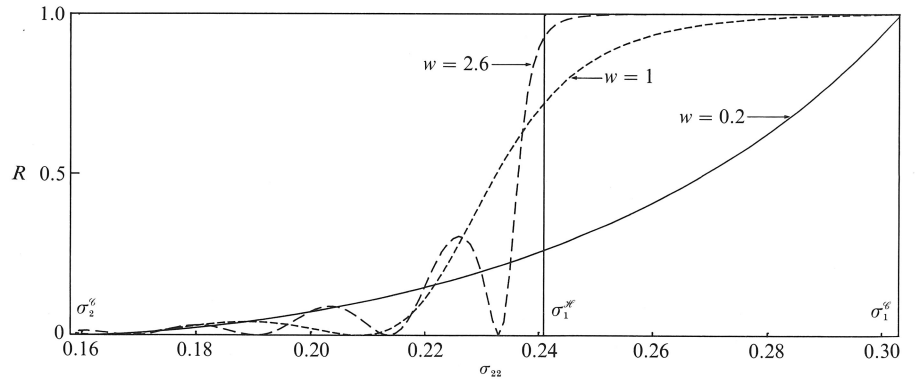

FIGURE 12. The reflection coefficient as a function of the frequency of the incident fundamental wave for three values of the headland width. Waves are not propagating abreast the headland for $\sigma > \sigma_1^{\mathscr{H}}$. The parameters are $N = 8$, $b = 1$, $r = 1$, $l = 0.22$.

and hardly any enters the estuary. For particular frequencies, depending on the geometry and the topography, perfect reflection occurs and the incident shelf wave generates a strong wave field in the estuary, figure 10(*b*, *c*). This is demonstrated in figure 11, showing the estuary energy as a function of the incident shelf wave frequency. These resonances can be attributed to trapped modes in the estuary; their stream function is displayed in figures 7(*c*) and 10(*c*), respectively.

3.4. *Scattering by a headland*

Again frequencies $\sigma > \sigma_2^{\mathscr{C}}$ are considered, so only the first mode is propagating in the channel. The scattering region is taken to be a headland of width w and length l with $0 \leqslant l < \frac{1}{2}$ so $\sigma_2^{\mathscr{C}} < \sigma_1^{\mathscr{H}} < \sigma_1^{\mathscr{C}}$. At frequencies σ where $\sigma_2^{\mathscr{C}} < \sigma < \sigma_1^{\mathscr{H}}$ only the fundamental propagates abreast the headland. At higher frequencies where $\sigma_1^{\mathscr{H}} < \sigma < \sigma_1^{\mathscr{C}}$ all waves abreast the headland are evanescent. Figure 12 shows the reflection coefficient for a mode-1 wave incident from $x = -\infty$ onto the headland as a function of the frequency. The headland cutoff $\sigma_1^{\mathscr{H}}$ is indicated by a vertical line. For $\sigma > \sigma_1^{\mathscr{H}}$ part of the wave energy tunnels through the headland region and appears as an

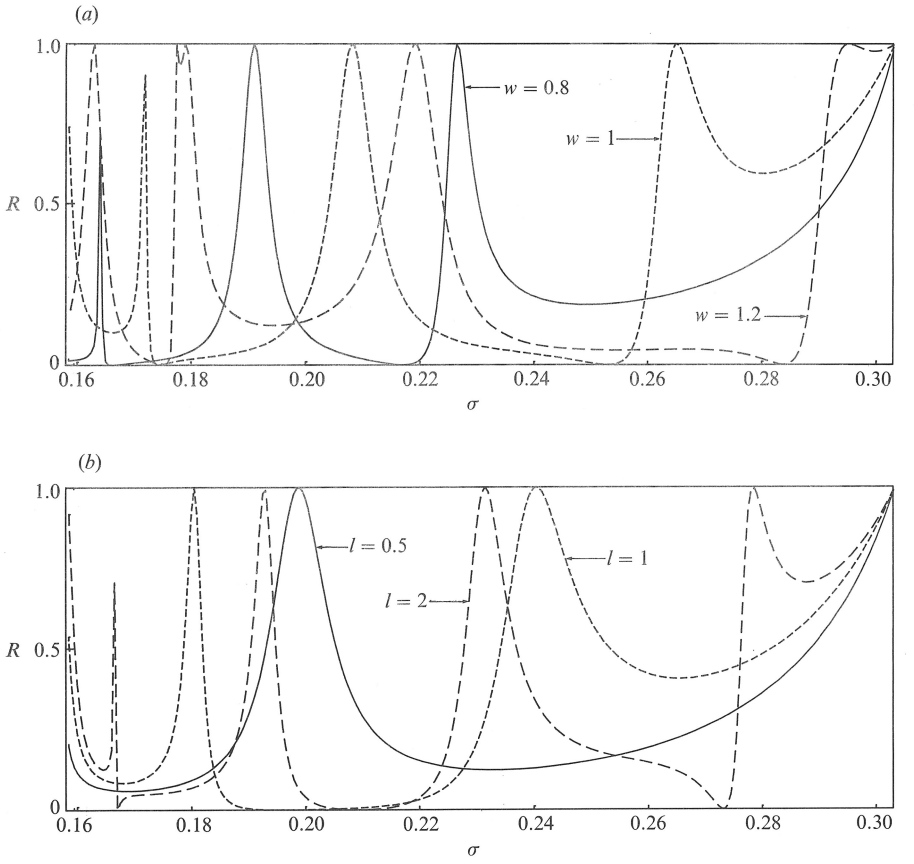

FIGURE 9. The reflection coefficient as a function of the incident wave frequency in a shelf–estuary system: (*a*) for three values of the estuary width with $l = 1.5$; and (*b*) three values of the estuary length with $w = 1$. The parameters are $N = 8$, $b = 1$, $r = 1$.

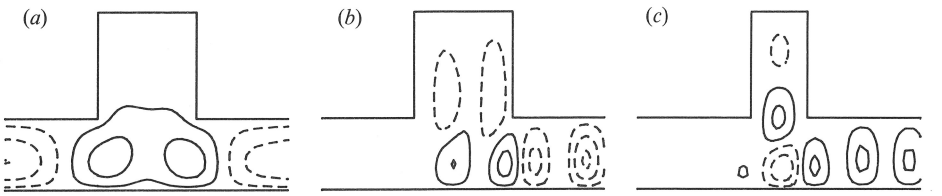

FIGURE 10. Streamlines for (*a*) perfect transmission and (*b*, *c*) perfect reflection or resonance of incident wave energy. The parameters are $N = 16$, $b = 1$, $r = 1$, $l = 1.5$; (*a*) $w = 1.4$, $\sigma = 0.262$, (*b*) $w = 1.5$, $\sigma = 0.204$ and (*c*) $w = 0.8$, $\sigma = 0.191$.

the estuary. Increasing estuary length similarly results in more and higher frequencies of perfect reflection. Generally, decreasing the area of the scattering region reduces the reflection coefficient. Most of the incident wave energy is transmitted when the estuary is much narrower or shorter than the shelf width. Figure 9(*a*, *b*), however, also indicates that for any geometry of the estuary there exist frequency bands with almost complete transmission or almost complete reflection.

Contours of the stream function are displayed in figure 10. In figure 10(*a*) there is no scattering: all incident wave energy is transmitted to the other side of the estuary

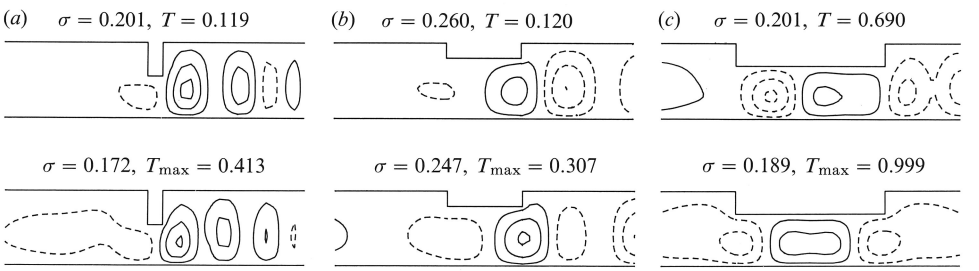

FIGURE 13. Streamlines for an incident fundamental wave tunnelling past a headland region with (*a*) $w = 0.2$, $l = 0.45$, and (*b*) $w = 1$, $l = 0.2$, and (*c*) propagating past a headland with $w = 2$, $l = 0.3$. The parameters are $N = 16$, $b = 1$, $r = 1$.

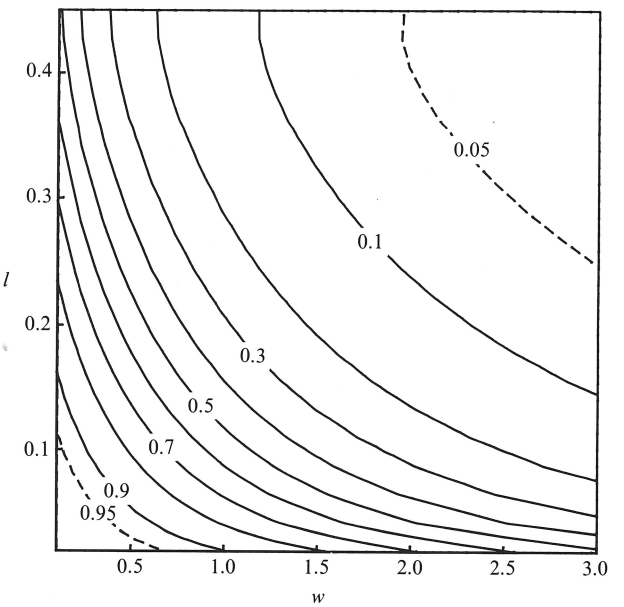

FIGURE 14. Contours of the maximum transmission coefficient of an incident fundamental wave tunnelling through the region abreast a headland as a function of headland width w and length l. The parameters are $N = 16$, $b = 1$, $r = 1$.

attenuated shelf wave on the far side. The amount of tunnelled energy increases as the frequency approaches $\sigma_1^{\mathscr{H}}$ since the e-folding length of the lowest evanescent modes increases. A wider headland reduces transmission. If waves can propagate in the zone abreast the headland most of the energy can be transmitted. It is remarkable that at particular frequencies the incident wave passes the scattering region undisturbed and no energy is reflected. On the other hand, perfect reflection of wave energy does not occur. The number of frequencies where $T = 1$ increases with increasing headland width. The headland acts as a filter, passing waves with particular frequencies according to the geometry and topography of the headland.

Tunnelling modes are shown in figure 13 for a narrow and long (*a*) and a wide and short (*b*) headland. Solutions with weak tunnelling ($T = 0.12, \sigma > \sigma_1^{\mathscr{H}}$) and maximum tunnelling ($\sigma = \sigma_1^{\mathscr{H}}$) are compared. Figure 13(*c*) displays solutions propagating abreast the headland with partial transmission (above) and perfect transmission (below).

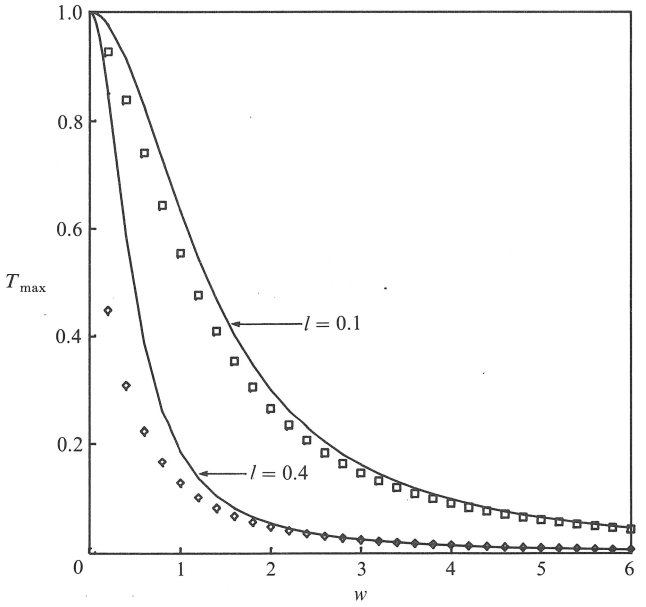

FIGURE 15. The maximum transmission coefficient T_{max} of tunnelled wave energy as a function of the headland width. T_{max} approaches the values obtained from one-dimensional wave mechanics for large w (solid lines). The parameters are $N = 8$, $b = 1$, $r = 1$.

The transmission coefficient takes a maximum, i.e. $T = T_{max}$, for $\sigma = \sigma_1^{\mathscr{H}}$ where $\lambda_1^{\mathscr{H}} = 0$ and the e-folding length of the first headland mode goes to infinity. The dependence of T_{max} on the geometric parameters w and l is shown in figure 14. Increasing the area of the scattering region decreases transmission if waves cannot propagate there.

The asymptotic behaviour of T_{max} for large widths w is given by

$$T_{max} \approx [1 + (\tfrac{1}{2}\kappa_1 w)^2]^{-1} \quad (\kappa_1 w \gg 1). \tag{3.3}$$

This result follows from one-dimensional wave mechanics (Landau & Lifshitz 1965) for a particle/wave travelling on a straight line. The transmission coefficient of an incident particle scattered by a constant potential barrier is calculated by solving the Schrödinger equation. The length of the potential barrier is w, and its strength exactly balances the kinetic energy of the incoming particle with wavenumber κ_1 (a classical particle would be completely reflected). Figure 15 gives T_{max} as a function of w for two headland lengths, and κ_1 is given by (2.7) with σ replaced by $\sigma_1^{\mathscr{H}}$. The solid lines show the result from one-dimensional theory, which is a good approximation for $w > 2\pi/\kappa_1 = 4.1$ for $l = 0.1$ with $\sigma_1^{\mathscr{H}} = 0.275$, and $w > 1.5$ for $l = 0.4$ with $\sigma_1^{\mathscr{H}} = 0.188$. The decay of T_{max} with increasing headland width is slower than exponential. Equation (3.3) provides a simple estimate of the maximum amount of energy that can be tunnelled past a headland if the width exceeds the wavelength of the incoming shelf wave.

3.5. *Conformally equivalent geometries*

Equation (2.1) is invariant under conformal mappings (Davis 1983) and so the present results have much wider applicability. In particular the estuary and headland geometries can be mapped to channels of constant width containing respectively a submerged ridge (figure 16*a*) or a submerged valley (figure 16*b*).

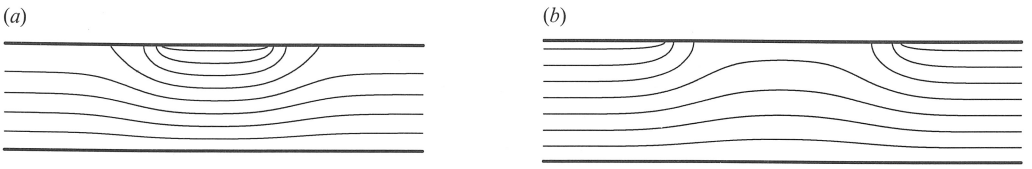

FIGURE 16. Constant-width channels with bathymetry conformally equivalent to the geometries studied above. (*a*) A submerged ridge corresponding to an estuary with $r = 1$, $l = 0.6$, $w = 1$. (*b*) A submerged valley corresponding to a headland with $r = 1$, $l = 0.5$, $w = 1$.

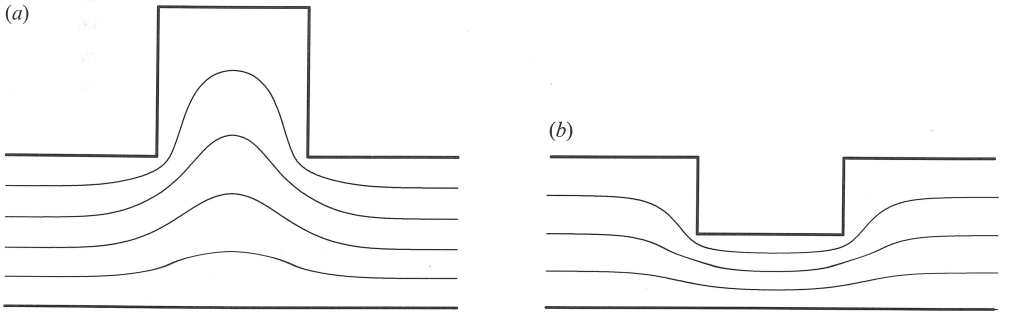

FIGURE 17. Bathymetries allowing transmission of energy at all frequencies without scattering. (*a*) An estuary with $r = 1$, $l = 1$, $w = 1$. (*b*) A headland with $r = 1$, $l = 0.5$, $w = 1$.

Although explicit formulae for the derivatives of the required transformation for this figure and figure 17 can be obtained as a Schwartz–Christoffel mapping, the transformations themselves have no simple closed forms. However, here and also in more complicated geometries, isobaths of equivalent geometries follow easily by solving finite-difference approximations to Laplace's equation. The solution given in the preceding sections then shows that submerged ridges support trapped modes, cause strong scattering and at certain frequencies can reflect or transmit all incoming energy. Submerged valleys can transmit energy even when they support no propagating modes.

As the topography has been constrained to be rectilinear in the analysis to date, discussion of the results has been in terms of the width and length of the estuary or headland. The shape of the bottom contours is equally important and, in particular, for a given boundary shape there is always a bathymetry allowing waves at all frequencies to pass without scattering. This can be constructed by conformally mapping the bathymetry for a rectilinear channel to the required geometry (Johnson 1987). Figure 17 (*a*, *b*) gives bathymetries with a rectangular estuary or headland but no scattering of shelf waves at any frequency. Scattering depends on the shape of both the coastline and the isobaths. In general shelf waves are not scattered if irrotational flow is geostrophic (Johnson 1989*c*).

4. Discussion

The trapping and scattering of topographic waves by large abrupt coastal irregularities has been investigated by modelling an interrupted shelf by a channel with a rectangular estuary or headland. Solutions of the non-divergent, linear barotropic equations for the conservation of potential vorticity are obtained by superposing modes of increasing transverse order. The relative amplitudes of the modes follow from requiring the velocity to be continuous. This yields a system of

linear algebraic equations. This system is considerably reduced by using a purely real formulation incorporating the symmetry of the geometry. Converging numerical solutions are obtained by truncating the system to finite order.

The depth change across the estuary region is greater than that across the adjoining channel and so the cutoff frequency for propagating waves is higher in the estuary. As shown in recent studies (Stocker 1988; Stocker & Johnson 1989) this leads to modes propagating in the estuary and exponentially evanescent outside. While trapped modes in semi-infinite channels only occur in a certain range of values of the topography and geometry parameters (Stocker & Johnson 1989), this is not the case in the present bathymetry: trapped modes can always be found in the neighbourhood of the estuary. A general reason for this difference follows from bounds presented for the various eigenfrequencies. If a region of a shelf has a higher cutoff frequency than its neighbouring regions, then at least one trapped mode is supported there. For estuaries of width of the order the shelf width, wave motion is localized in the estuary and round the estuary mouth. When the estuary becomes narrower, wave energy no longer enters the estuary but is concentrated on the shelf. At the same time, the eigenfrequency approaches the cutoff frequency of freely propagating shelf waves. In the extreme case of a very narrow estuary or inlet this yields modes trapped on the shelf at the entrance of the inlet with a frequency slightly higher than the cutoff. This leads to the prediction that mouths of bays or estuaries should exhibit significant non-propagating horizontal kinetic energy at periods just shorter than the cutoff of the shortest-period shelf wave.

The study has further shown that an incident propagating wave is scattered into a reflected and a transmitted wave through a process strongly dependent on the geometry of the scattering region and the frequency of the incident wave. For many values of the relevant parameters most incident energy is transmitted: the incident wave propagates past the estuary mouth with little interaction. At some frequencies transmission is perfect and an incident wave does not interact with the estuary. At some other frequencies all energy is reflected and none is transmitted to the shelf beyond the estuary mouth. This coincides with a resonance when the wave field influences appreciably the interior of the estuary.

Solutions for the complementary geometry of a channel interrupted by a rectangular headland are also given. Here no trapped modes are possible as the cutoff frequency of waves abreast the headland is lower than in the channel. Incident waves of frequency σ, where $\sigma_1^{\mathscr{H}} < \sigma < \sigma_1^{\mathscr{C}}$, cannot propagate through the headland region; however, part of their energy always tunnels through this zone and appears as a weaker propagating wave on the far side of the headland. Wave energy observed after a region of no propagation is thus not necessarily locally generated; it may come from energy tunnelled through the zone of no propagation. The amount of tunnelled energy decreases with increasing area of the headland. The maximum value of the transmission coefficient $T_{\max}$ in the case of tunnelling occurs at the headland cutoff frequency $\sigma_1^{\mathscr{H}}$. For large headland widths scattering is essentially one-dimensional and $T_{\max}$ is a simple rational function of the ratio of headland width to incident wavelength. If waves propagate in the headland zone, little energy is reflected by the obstacle. For any width of the scattering region there exist particular frequencies at which transmission is perfect whereas total reflection never occurs.

Schwing (1989) reports observations of subtidal variations on the Scotian Shelf where it is interrupted by the Laurentian Channel (figure 1*a*). As in the present work he models his observations as barotropic, noting that the non-local response is consistent with theoretical estimates of first- and second-mode shelf waves and

represents direct evidence for shelf wave activity on the Scotian Shelf. Unlike the results above, the theory presented by Schwing also requires the long-wave and low-frequency approximations and so cannot discuss trapped modes. In describing the observations, however, Schwing notes that significant energy is present in the neighbourhood of the estuary mouth, both at Port aux Basques on the Newfoundland side of Cabot Strait and at Louisbourg on the shelf, away from the strait but near the channel–shelf junction. Schwing comments that energy at this frequency (0.563 cycles per day) cannot be propagating effectively as it is absent from the spectral distribution at Whitehead Harbour, only 140 km west of Louisbourg. The observations may thus be a manifestation of a mode trapped in the estuary and evanescent on the shelf away from the estuary mouth. In further accord with the results on trapped modes in §3.2, note that the frequency of the energy in the estuary is higher than the dominant frequency (0.438 cycles per day) observed on the shelf away from the estuary (Whitehead Harbour, Sambro and West Head).

The three strongest approximations involved in modelling coastal flows by the vorticity equation (2.1) are the neglect of free-surface effects, dissipation and stratification. Taking the fluid to be constrained by a rigid lid filters out the free-surface Kelvin wave. This wave is present at all frequencies and so modes trapped when the surface is rigid may leak energy and be transformed to resonances. Energy can also be scattered between gravity and rotational modes. Such scattering will be considered elsewhere, although it follows from Buchwald & Adams (1968) and Middleton *et al.* (1987) that the disparity in scales between the Kelvin wave and shelf waves on many shelves means that coupling will be weak.

The present work considers only free modes. However, particularly in the shallow regions of estuaries, bottom friction will be important and incoming shelf wave energy can be dissipated. The neglect of dissipation on the shelf itself seems less serious. Schwing (1989) estimates an exponential decay at all frequencies of approximately 900 km in the direction of propagation, a distance large compared to estuary or headland widths. Dissipative effects can thus be expected to be negligible for trapped modes which, as shown by figure 5, are concentrated over the shelf at the estuary mouth: although the estuary determines the location of the trapped mode the dynamics are close to those of propagating shelf waves. The flows likely to be most strongly affected by dissipation are resonances like those shown in figures 7(*c*) or 10(*b*, *c*). Energy penetrates to the shallow end of the estuary and can be strongly dissipated there. The estuary continues to act as a complete barrier and no energy is transmitted at this frequency but the reflected short-wave energy may be considerably reduced in amplitude.

Results are derived here for barotropic flows. They thus apply directly to the well-mixed high-latitude shelves where Middleton *et al.* (1987) and Schwing (1989) obtained their data. However, the results would be modified significantly on steep, strongly stratified shelves. Wilkin & Chapman (1987) point out that for sufficiently strong stratification there are no short waves carrying energy in the opposite direct to the long waves, and long waves propagate at all sub-inertial frequencies. The trapped modes and resonances obtained here would then be absent. Nevertheless, provided the buoyancy is less than f times the average slope of the shelf, some sub-inertial waves remain evanescent (Huthnance 1978) and trapped modes are possible in a reduced band of frequencies.

One of the authors (T.F.S.) was supported by SERC grant GR/F11023 while performing this study. We are indebted to the referee of a previous draft of this paper

for his helpful comments, and to Dr D. G. Wright for drawing our attention to the paper by Dr Schwing whose observations accorded so well with the predictions of the previous draft.

REFERENCES

BUCHWALD, V. T. & ADAMS, J. K. 1968 The propagation of continental shelf waves. *Proc. R. Soc. Lond.* A **305**, 235–250.

BUCHWALD, V. T. & WILLIAMS, N. V. 1975 Rectangular resonantors on infinite and semi-infinite channels. *J. Fluid Mech.* **67**, 497–511.

DAVIS, A. M. J. 1983 Shelf-similar topographies for free continental shelf waves. *Geophys. Astrophys. Fluid Dyn.* **23**, 321–331.

GRIMSHAW, R. 1977 The effects of a variable Coriolis parameter, coastline curvature and variable bottom topography on continental shelf waves. *J. Phys. Oceanogr.* **7**, 547–554.

HUTHNANCE, J. M. 1978 On coastal trapped waves: analysis and numerical calculation by inverse iteration. *J. Phys. Oceanogr.* **8**, 74–92.

JOHNSON, E. R. 1987 A conformal-mapping technique for topographic-wave problems: semi-infinite channels and elongated basins. *J. Fluid Mech.* **177**, 395–405.

JOHNSON, E. R. 1989*a* Topographic waves in open domains. Part 1. Boundary conditions and frequency estimates. *J. Fluid Mech.* **200**, 69–76.

JOHNSON, E. R. 1989*b* Boundary currents, free currents and dissipation in the low-frequency scattering of shelf waves. *J. Phys. Oceanogr.* **19**, 1291–1300.

JOHNSON, E. R. 1989*c* Connection formulae and classification of scattering regions for low-frequency shelf waves. *J. Phys. Oceanogr.* **19**, 1301–1310.

JOHNSON, E. R. 1990 Low-frequency barotropic scattering on a shelf bordering an ocean. *J. Phys. Oceanogr.* (in press).

LANDAU, L. D. & LIFSHITZ, E. M. 1965 *Quantum Mechanics, Course in Theoretical Physics*, vol. 3, Pergamon, 616 p.

LIGHTHILL, M. J. 1958 *An Introduction to Fourier Analysis and Generalised Functions*. Cambridge University Press.

MYSAK, L. A. 1980 Recent advances in shelf wave dynamics. *Rev. Geophys. Space Phys.* **18**, 211–241.

MIDDLETON, J. H., FOSTER, T. D. & FOLDVIK, A. 1987 Diurnal shelf waves in the southern Weddell Sea. *J. Phys. Oceanogr.* **17**, 784–791.

MIDDLETON, J. H. & WRIGHT, D. G. 1988 Shelf wave scattering due to a longshore jump in topography. *J. Phys. Oceanogr.* **18**, 230–242.

SCHWING, F. B. 1989 Subtidal response of the Scotian Shelf bottom pressure field to meteorological forcing. *Atmos. Ocean* **27**, 157–180.

STOCKER, T. 1988 A numerical study of topographic wave reflection in semi-infinite channels. *J. Phys. Oceanogr.* **18**, 609–618.

STOCKER, T. & HUTTER, K. 1987 Topographic waves in rectangular basins. *J. Fluid Mech.* **185**, 107–120.

STOCKER, T. F. & JOHNSON, E. R. 1989 Topographic waves in open domains. Part 2. Bay modes and resonances. *J. Fluid Mech.* **200**, 77–93.

WEBSTER, I. 1987 Scattering of coastally trapped waves by changes in continental shelf width. *J. Phys. Oceanogr.* **17**, 928–937.

WILKIN, J. L. & CHAPMAN, D. C. 1987 Scattering of continental shelf waves at a discontinuity in shelf width. *J. Phys. Oceanogr.* **17**, 713–724.